ACS APPLIED MATERIALS & INTERFACES

www.acsami.org

Research Article

Functional Single-Walled Carbon Nanotubes for Anion Sensing

Seon-Jin Choi, Bora Yoon, Sibo Lin, and Timothy M. Swager*

Cite This: *ACS Appl. Mater. Interfaces* 2020, 12, 28375−28382

Read Online

ACCESS | Metrics & More | Article Recommendations | Supporting Information

ABSTRACT: We report an anion-sensing platform wherein conductance changes are triggered by chemical interactions between selectors and anions. The selector design incorporates both a cationic moiety (i.e., pyridinium) and a thiourea-based dual-hydrogen-bond donor. Anion binding by a model selector (**2**) was studied using ^{1}H NMR and UV−vis titrations, which reveal a binding strength toward acetate ions (AcO^-) followed by Cl^- > Br^- > NO_3^-. These studies reveal that selector **2** is deprotonated upon addition of AcO^-, whereas it undergoes hydrogen bonding associated with Cl^-, Br^-, and NO_3^-. The cationic pyridinium moiety improves anion binding affinity by lowering the pK_a value of selector **2** and enhancing the hydrogen-bond donor capability as confirmed by spectroscopic titrations and DFT calculations. The selector is covalently attached to poly(4-vinylpyridine) (P4VP), which wraps single-walled carbon nanotubes (SWCNTs) (i.e., P4VP-**2**-SWCNT) to transduce an electrical signal. As a result, continuous anion sensing was achieved with high sensitivity represented by a normalized resistance change of 101.9 ± 10.3% toward 16.7 mM AcO^-, whereas negligible sensitivity was observed toward Cl^-, Br^-, and NO_3^-. The sensitivity transition was attributed to the internal charge transfer of **2** by deprotonation of the thiourea proton upon addition of AcO^-.

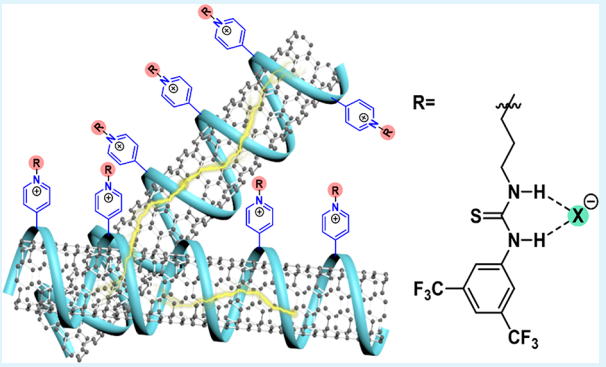

KEYWORDS: *single-walled carbon nanotubes, thiourea, anion sensing, pyridinium, chemiresistor*

INTRODUCTION

Determination of anion concentrations in aqueous solutions is central to environmental and healthcare technologies.[1−4] In particular, selective detection of acetate and chloride is widely needed in biotechnology and biomedical research.[5,6] The acetate anion (AcO^-) is, in particular, a metabolic switch regulating the growth of bacteria cells for production of recombinant proteins or food fermentation.[7−9]

Developments in anion recognition have advanced by addressing several issues associated with the intrinsic properties of anionic species including their large size, sensitivity to pH, and wide range of geometries.[3] Anion receptors or selectors employing hydrogen-bond donors have been extensively studied as a result of access to a wide range of geometrical variations and expedient synthesis procedures. Furthermore, dual-hydrogen-bond donors with directional H bonds have been shown to be highly effective with Y-shaped anions such as AcO^- and benefit from geometrical chelation effects and preorganization.[10] The (thio)urea group is the basis of many dual-hydrogen-bond donors that provide high anion binding affinity and selectivity employing directional binding interactions.[11−13] In addition, deprotonation of the −NH protons of acidic (thio)urea receptor was observed upon addition of basic anions such as fluoride (F^-) and AcO^-.[14] A recent comprehensive review summarized *N*,*N*′-substituted (thio)urea-based receptors for anion complexation and sensing,[15] and another recent publication highlighted metal-coordinated (thio)urea receptors for binding of oxyanions such as nitrate (NO_3^-), sulfate (SO_4^{2-}), and dihydrogen phosphate ($H_2PO_4^-$).[10]

To detect anions with high sensitivity and lower the detection limits, there has been significant progres in terms of the development of anion-selective ionophores utilizing various types of interactions including coordination to a metal center, ion pairing, electrostatics, and hydrogen bonding.[16−22] In particular, receptors utilizing hydrogen-bond interactions and deprotonation have been exploited for the development of chemosensors using fluorescence,[23−26] colorimetric,[27,28] and electrochemical transduction.[29−33] However, weak hydrogen-bond interactions are often ineffective at the binding of anions in aqueous conditions. A general approach to overcome this limitation has been to use combinations of electrostatic and hydrogen-bonding interactions to synergistically attract anions. Positively charged interfacial layers have been shown to alter the solvation structure at the interface or the monolayer ordering upon adsorption of a certain anion in the presence of water.[34,35] For this reason, anion receptors containing cationic

Received: February 28, 2020
Accepted: May 28, 2020
Published: June 10, 2020

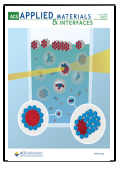

https://dx.doi.org/10.1021/acsami.0c03813
ACS Appl. Mater. Interfaces 2020, 12, 28375−28382

moieties such as imidazolium,[36,37] triazolium,[38] pyridinium,[39] and multivalent cationic ligand[40,41] have found utility in aqueous solvent mixtures.

Spectroscopic methods such as ^{1}H NMR and UV−vis titrations are used to reveal details of binding mechanisms[42] as well as equilibrium constants. However, these standard analytical methods are not well suited for rapid screening and on-site detection of anions in environmental and biological samples. For this reason, development of portable anion sensors with rapid identification of anion species is needed for real-time analysis.

Carbon nanotube-based chemiresistive sensors for gaseous analytes have proven to be sensitive, rapid, and simple to operate.[43,44] To develop a real-time anion sensor with stable electrical transduction in solution, chemical anchoring of the carbon nanotube layer onto a substrate is essential to prevent detachment during the sensing process. In our previous studies, we reported mechanically robust anchoring of single-walled carbon nanotubes (SWCNTs) by wrapping with poly(4-vinylpyridine) (P4VP), wherein the P4VP forms a covalent bond on a surface-treated glass substrate by quaternization reaction.[45−47] The residual pyridyl groups from P4VP represent active sites for further functionalization of anion selector to induce anion binding interactions. We previously demonstrated the anion-sensing properties by functionalization of suquaramide-based selector on the residual pyridyl groups, which confirms conductance changes as a result of the deprotonation of squaramide upon interactions with anions.[48]

Herein, we report the versatility of our chemiresistive anion sensors based on SWCNTs by noncovalent functionalization of thiourea-based dual-hydrogen-bond donor and cationic pyridinium. The chemiresistive-sensing mechanism provides for high sensitivity, the origins of which were determined by detailed studies of the anion binding. Three chemiresistors were assembled for sequential detection of multiple anions in real time.

RESULTS AND DISCUSSION

Our anion-sensing platform makes use of a chemiresistive signal transduction that responds to addition of anions to a solution (Figure 1). Surface anchoring of P4VP-wrapped SWCNTs (P4VP-SWCNT) creates a mechanically stable sensing layer by quaternization of pyridyl groups from P4VP with alkyl bromides on a surface-treated glass substrate.[45−47] Subsequently, the residual pyridyl groups from the P4VP are functionalized with thiourea-containing groups, resulting in formation of cationic pyridinium moieties proximate to the recognition elements. Changes in resistance were evaluated in real-time upon addition of anion species, wherein the electrical signal is triggered by the binding of anions (X^-) to the thiourea-based selector.

To understand the binding affinity of the thiourea-based selector, we synthesized a model structure (Scheme S1 in the Supporting Information). Briefly, 1-(3-ammoniumpropyl)-pyridinium dibromide (**1**) was prepared by the reaction between 3-bromopropylamine hydrobromide (2 g, 9.14 mmol) and pyridine (490 μL, 6.09 mmol) in refluxing anhydrous acetonitrile for 24 h. Subsequently, the thiourea group with an electron-withdrawing 3,5-bis(trifluoromethyl)phenyl group (**2**) was obtained by reaction of **1** (100 mg, 0.34 mmol), 3,5-bis(trifluoromethyl)phenyl isothiocyanate (75 μL, 0.40 mmol), and triethylamine (140 μL, 1.01 mmol) in MeOH (10 mL).

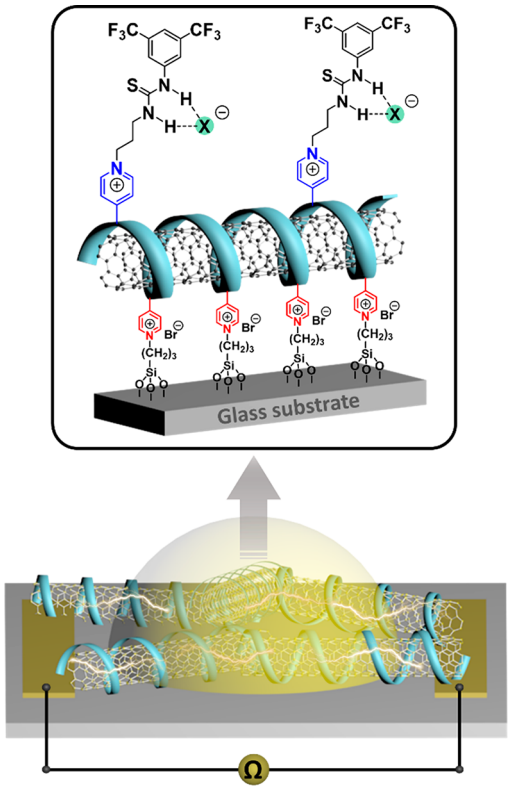

Figure 1. Schematic illustration of the anion-sensing platform with P4VP-SWCNT functionalized with thiourea-based selector **2**.

The anion binding affinity of selector **2** was investigated by ^{1}H NMR titrations under sequential addition of anions including AcO^-, chloride (Cl^-), bromide (Br^-), and NO_3^- in the concentration range of 0−3.60 equivalents. Downfield movement of chemical shifts ($\Delta\delta$) up to 3.18 ppm (from 10.32 to 13.50 ppm) and broadening of the N−H proton (H_α) were observed upon addition of 3.22 equiv of AcO^- (Figure 2a). The broadening of the H_α peak is mainly attributed to the deprotonation as a result of the enhanced hydrogen-bond donation of H_α located in the proximity of the electron-withdrawing 3,5-bis(trifluoromethyl)phenyl group.[49] In addition, the aromatic proton H_γ experienced a noticeable downfield shift ($\Delta\delta$ = 0.09 ppm) after addition of 3.22 equiv of AcO^-. This perturbation implies that the cationic pyridinium group contributes to the binding affinity of AcO^-, perhaps via a folded conformation of the selector **2**. Similarly, anion binding properties toward Cl^-, Br^-, and NO_3^- were investigated by ^{1}H NMR titrations (Figures S1−S3), and the chemical shifts are summarized in Figure 2b. There was a noticeable change in the chemical shift of H_α ($\Delta\delta$ = 0.79 ppm) upon addition of 3.53 equiv of Cl^- (Figure S1). However, only minor changes ($\Delta\delta \leq 0.15$ ppm) were observed toward Br^- and NO_3^-. The binding stoichiometry between **2** and AcO^- was investigated by completing a Job plot (a continuous variation method) wherein aliquots of the AcO^- solution are added to the solution of selector **2** and chemical shifts as an analytical signal are monitored throughout the process. The result revealed that selector **2** and AcO^- exhibit 1:1 complex binding stoichiometry (Figure 2c). Equilibrium constants (K) were calculated by plotting chemical shifts versus the equivalent of anions in Figure 2 and are summarized in Table 1. Equilibrium constants for AcO^- (1.99×10^3 M^{-1})

https://dx.doi.org/10.1021/acsami.0c03813
ACS Appl. Mater. Interfaces 2020, 12, 28375−28382

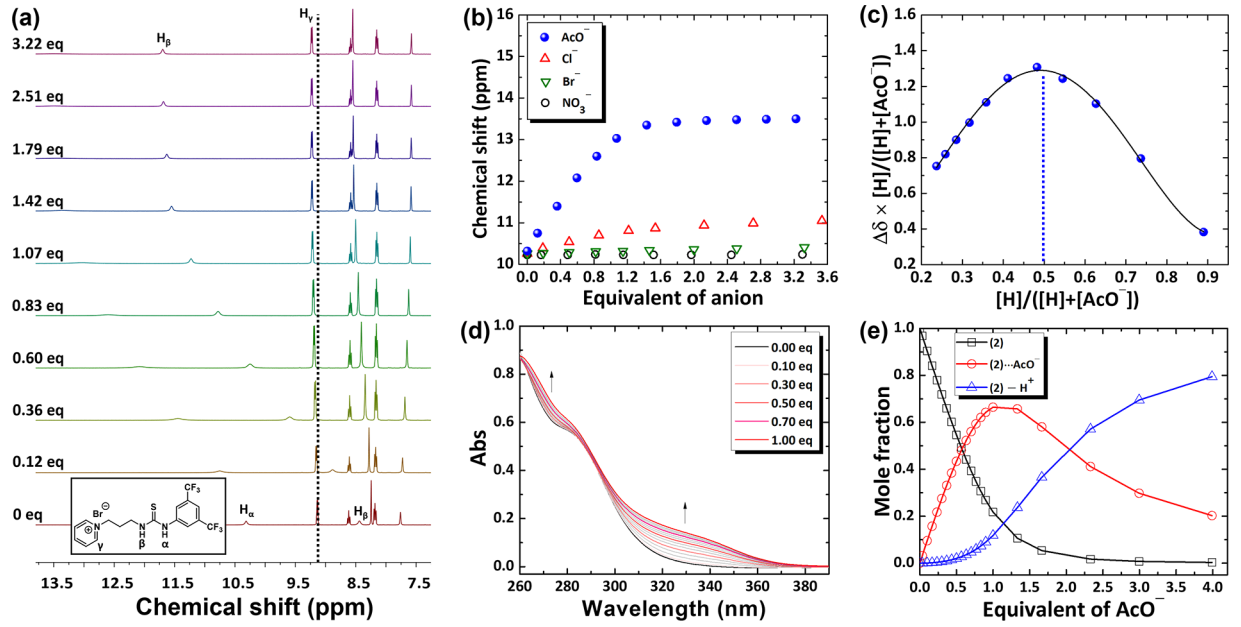

Figure 2. (a) Transitions of ^{1}H NMR spectra of the selector **2** ([**2**] = 1.2 × 10^{-2} M) upon addition of AcO$^-$ in the range of 0−3.2 equiv in DMSO-d_6 (dashed line is the chemical shift of H$_\gamma$ at 0 equiv of AcO$^-$). (b) Chemical shifts of the N−H proton (H$_\alpha$) upon addition of AcO$^-$, Cl$^-$, Br$^-$, and NO$_3^-$ in DMSO-d_6. (c) Job plot of selector **2** based on ^{1}H NMR titrations in DMSO-d_6 upon addition of AcO$^-$. (d) UV−vis titrations of selector **2** ([**2**] = 4.11 × 10^{-5} M) by addition of AcO$^-$ in the range of 0−1 equiv in DMSO. (e) Mole fractional transitions of selector **2** and corresponding complexes with respect to the sequential addition of AcO$^-$.

Table 1. Equilibrium Constants K [M^{-1}] Determined by ^{1}H NMR titrations in DMSO-d_6 at 298 K[a]

	anion X$^-$	AcO$^-$	Cl$^-$	Br$^-$	NO$_3^-$
selector **2**	K (H$_\alpha$) [M^{-1}]	1.99 × 10^3	2.51 × 10^2	14.16	1.66 × 10^{-4}
	$\Delta\delta$	3.18	0.79	0.15	0.01

[a]Anions were added as tetrabutylammonium salts. Chemical shifts ($\Delta\delta$) were calculated based on the shifts of the H$_\alpha$ proton after the addition of >3 equiv of anion. Estimated error in K < 15%.

and Cl$^-$ (2.51 × 10^2 M^{-1}) were obtained using selector **2**, whereas relatively low equilibrium constants less than 15 M^{-1} were observed for Br$^-$ and NO$_3^-$ (Table 1).

UV−vis titrations were performed with **2** to further investigate the binding properties upon addition of AcO$^-$ in DMSO (Figure 2d and Figure S4). There was a noticeable enhancement in the absorbance intensity at around 330 nm upon addition of 1 equiv of AcO$^-$. The absorbance changes at 330 nm with respect to the mole fractional transitions of the hydrogen-bonded complex (i.e., **2**···AcO$^-$) revealed 1:1 binding stoichiometry with 66% hydrogen-bonding interaction after the addition of 1 equiv of AcO$^-$ (Figure 2e). The decreased mole fraction of **2**···AcO$^-$ beyond addition of 1 equiv was attributed to deprotonation of **2** and formation of a hydrogen-bond self-complex, i.e., [H(AcO)$_2$]$^-$.[50] UV−vis titrations of **2** upon addition of tetrabutylammonium hydroxide (TBAOH) were performed to sequentially deprotonate the selector **2** (Figure S5). Increasing absorption spectra were observed at 328 nm upon addition of TBAOH, which suggests that the characteristic absorbance changes around 330 nm after addition of AcO$^-$ were mainly attributed to deprotonation of **2**.[51]

To confirm the effect of the cationic pyridinium moiety on the anion binding strength, reference selector **3** was synthesized by replacing the pyridinium group with a hydroxyl group (Scheme S2 in the Supporting Information). Similarly, the binding affinity was investigated by ^{1}H NMR titrations under sequential addition of AcO$^-$ (0−2.72 equiv) (Figure S6). A large chemical shift change ($\Delta\delta$ = 3.01, from 10.06 to 13.07 ppm) of H$_\alpha$ was observed upon addition of 2.72 equiv of AcO$^-$. Job plot analysis confirmed that selector **3** exhibited 1:1 binding stoichiometry. The equilibrium constant of **3**, calculated based on the binding stoichiometry and change in chemical shift of H$_\alpha$ proton, was determined to be 7.10 × 10^2 M^{-1}. Although selector **3** can form a hydrogen bond between the terminal OH group and anions, a 2.8-fold enhanced AcO$^-$ binding affinity was achieved with the cationic selector **2** as compared to selector **3** (Table S1). In addition, UV−vis titrations with **3** confirmed a reduced AcO$^-$ binding affinity relative to **2**, wherein selector **3** forms largely a hydrogen-bond complex with AcO$^-$ rather than deprotonation of the thiourea group (Figure S7 and Table S2). Interestingly, 1:2 binding stoichiometry was observed for selectors **2** and **3** based on the Job plots determined by UV−vis titrations in DMSO at 330 nm upon addition of AcO$^-$ (Figure S8), which is mainly attributed to the diluted concentration of selectors in UV−vis titrations. We also confirmed the equilibrium constants of selectors **2** and **3** obtained by ^{1}H NMR titrations with a 1:2 binding mode, which revealed higher equilibrium constants for selector **2** as compared to the constants of selector **3** (Table S3).

The binding of selector **2** to various anions was investigated theoretically using density functional theory (DFT) calculations (See Supporting Information). The free energy changes were calculated by the replacement of counteranion (Br$^-$) in the model selector **2** with the analyte anions (X$^-$) (Figure 3a).

https://dx.doi.org/10.1021/acsami.0c03813
ACS Appl. Mater. Interfaces 2020, 12, 28375−28382

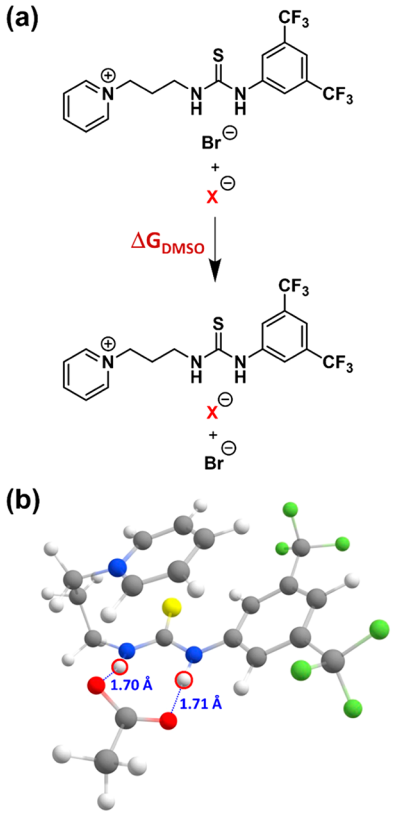

Figure 3. (a) Model structure of selector **2** before and after anion complex for calculation of the free energy change (ΔG) in DMSO. (b) Optimized geometry by DFT calculations for the complex of selector **2** with AcO^-.

Selector **2** exhibited a strong binding affinity toward AcO^- (ΔG = −3.8 kcal/mol) in DMSO and relatively weak binding interactions with Cl^- (ΔG = −1.1 kcal/mol). There was negligible interaction with NO_3^- ($\Delta G \approx$ 0.0 kcal/mol) in DMSO (Table 2). The calculated result supports the experimental observations, wherein selector **2** exhibited stronger binding affinity toward AcO^- as compared to the affinity to Cl^- and NO_3^-. To investigate the contribution of a cationic moiety (pyridinium) on the binding affinity, selector **3** was also studied with DFT calculations (Figure S9). Selector **3** exhibited less favorable binding to AcO^-, Cl^-, and NO_3^- as compared to the free energy changes of **2** (Table 2). In particular, selector **3** only binds AcO^- with ΔG = −1.6 kcal/mol. This result demonstrates the significant contribution of the pyridinium group to AcO^- binding. The optimized O−H distances between the N−H protons of **2** and the oxygen atoms of AcO^- were in the range of 1.70−1.71 Å (Figure 3b). In addition, in the computationally optimized structure the pyridinium of selector **2** is located above and parallel to the AcO^-, which illustrates the effect of pyridinium on AcO^- binding. In contrast, calculations with selector **3** and AcO^- revealed hydrogen-bonding H−O distances in the range of 1.71−1.77 Å (Figure S9), which is the result of weaker hydrogen-bond interactions when pyridinium is not present.

Table 2. Free Energy Changes (ΔG) of the Selectors after Binding with Anions in DMSO Obtained by DFT Calculations

	ΔG [kcal/mol]	
anion X^-	selector **2**	selector **3**
AcO^-	−3.8	−1.6
Cl^-	−1.1	−1.0
NO_3^-	~0.0	4.9

The anion binding strength was further investigated by measuring the Brønsted acidity (pK_a) of the selectors as the binding affinity is related to the hydrogen-bond donor capability of the thiourea group. The acidity of the selectors was evaluated by UV−vis titrations in DMSO (See Supporting Information).[52] The results reveal that selector **2** exhibited a lower pK_a value of 11.07 ± 0.11 as compared that of selector **3** (pK_a = 11.69 ± 0.07) (Figures S10 and S11). This is consistent with selector **2** exhibiting stronger binding affinities than selector **3**. Reasonable approximations for the experimental pK_a values of the selectors were achieved as confirmed by DFT calculations (Scheme S3 in the Supporting Information), wherein the calculated pK_a values exhibited differences of less than 1 pK_a unit (Table S4).

Incorporation of selector **2** into P4VP-SWCNT (P4VP-**2**-SWCNT) was achieved by the two-step surface reactions (Scheme S4 in the Supporting Information). Briefly, a thin line pattern of P4VP-SWCNT was fabricated on parallel electrodes by the spray-coating technique (Figure 4a). Four parallel sensing electrodes (E_1−E_4) form three series resistors (R_1−R_3), which constitute an anion sensor array for detection of multiple anions in series. Scanning electron microscopy (SEM) confirmed a width of 422 μm for the patterned P4VP-SWCNT. Subsequently, the quaternization of residual P4VP pyridyl groups was performed in a solution containing 3-bromopropylamine hydrobromide. After reaction with isothiocyanate, P4VP-**2**-SWCNT was obtained composed of a pyridinium moiety and a thiourea-based dual-hydrogen-bond donor with the electron-withdrawing 3,5-bis(trifluoromethyl)-phenyl group.

The functionalization steps were investigated by ATR-FTIR spectroscopy and X-ray photoelectron spectroscopy (XPS) (Figure 4b and 4c). The characteristic peak related to pyridine of as-sprayed P4VP-SWCNT was observed at 1598 cm^{-1} in the ATR-FTIR spectrum (Figure 4b). After quaternization this peak shifted to 1642 cm^{-1}.[53] In addition, the characteristic peak at 1280 cm^{-1} was attributed to the stretching vibrational mode of N−C═S from the thiourea group in P4VP-**2**-SWCNT.[54] The high-resolution XPS N 1s spectrum of P4VP-**2**-SWCNT revealed two characteristic peaks at 399.9 and 402.3 eV corresponding to the nitrogen from the amide group and pyridinium, respectively (Figure 4c). The N 1s spectra of P4VP-**2**-SWCNT and the model selector **2** exhibited almost identical peak information (Figure S12), which confirms the incorporation of selector **2** after the two-step surface reaction sequence. To prevent signal distortion and isolate the sensing region, a polydimethylsiloxane (PDMS) mold having cylindrical chambers is attached to the sensor substrate and the sensing solution was introduced into the chambers (see Supporting Information).

Real-time anion-sensing properties were investigated by measuring resistance changes upon addition of analytes including AcO^-, Cl^-, Br^-, and NO_3^- (Figure 5). Acetonitrile as the sensing solvent was used to obtain stable sensing characteristics instead of DMSO because the functionalized P4VP was dissolved in DMSO, resulting in reliability and reproducibility issues of the P4VP-**2**-SWCNT sensors. The sensitivity is defined as $[(R - R_0)/R_0]$ (%), where R_0 and R are

https://dx.doi.org/10.1021/acsami.0c03813
ACS Appl. Mater. Interfaces 2020, 12, 28375−28382

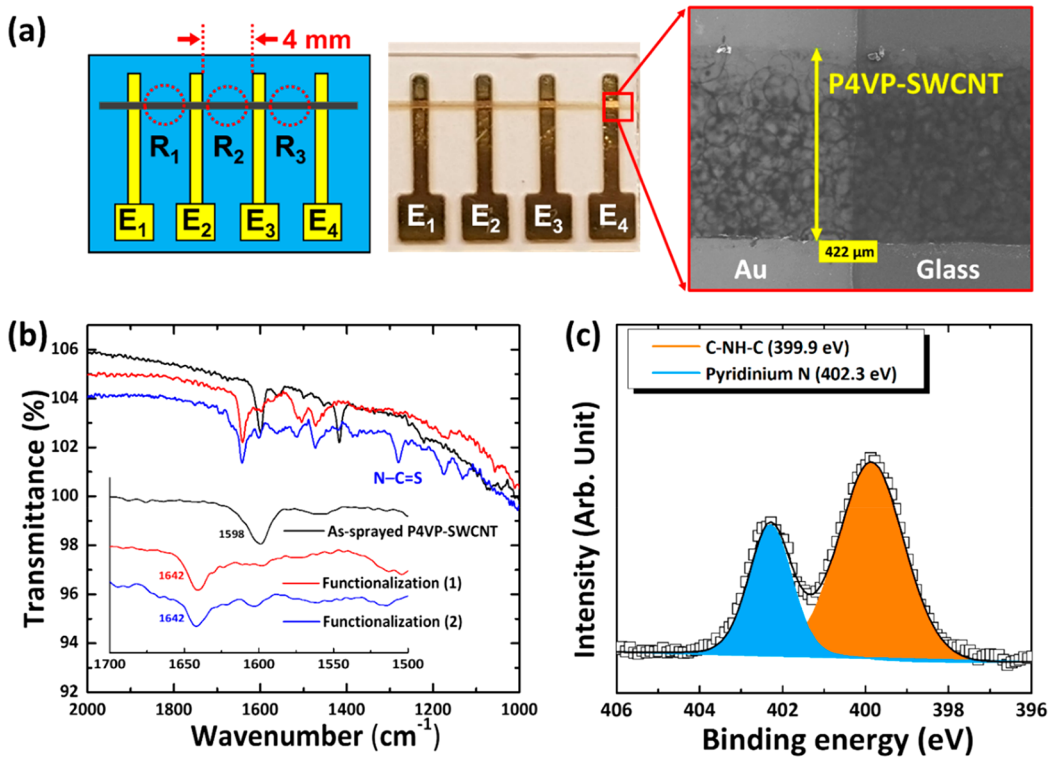

Figure 4. (a) Photograph of patterned P4VP-SWCNT across the parallel Au-sensing electrodes with the corresponding schematic illustration and scanning electron microscopy (SEM) image of the patterned P4VP-SWCNT on the substrate. (b) ATR-FTIR spectra of the P4VP-SWCNT with two-step functionalization on a glass substrate. (c) High-resolution X-ray photoelectron spectroscopy (XPS) N 1s spectrum of the P4VP-**2**-SWCNT.

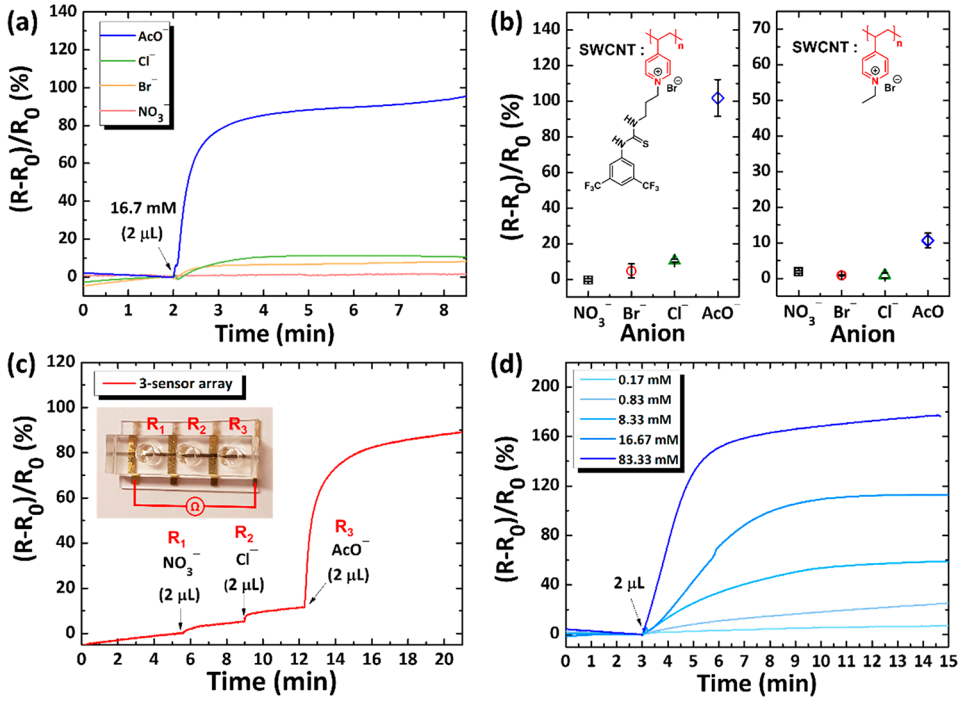

Figure 5. (a) Dynamic sensitivity transitions of the P4VP-**2**-SWCNT sensor toward AcO^-, Cl^-, Br^-, and NO_3^- after addition of 2 μL (16.7 mM) of analyte. (b) Comparison of sensitivity changes between P4VP-**2**-SWCNT and the ethylated P4VP-SWCNT toward AcO^-, Cl^-, Br^-, and NO_3^- under addition of 2 μL (16.7 mM) of analyte. (c) Real-time and sequential detection of multiple anions. (d) Dynamic sensitivity transitions of P4VP-**2**-SWCNT after addition of 2 μL of AcO^- in the concentration range of 0.17−83.33 mM.

the resistances of a sensor under exposure to baseline acetonitrile (10 μL) and analyte anion solution (2 μL), respectively. Dynamic sensitivity changes were evaluated by injection of analytes after stabilization of the P4VP-**2**-SWCNT

https://dx.doi.org/10.1021/acsami.0c03813
ACS Appl. Mater. Interfaces 2020, 12, 28375−28382

sensor in acetonitrile (Figure 5a). Rapid increases in resistance were observed after injection of 2 μL (16.7 mM) of AcO^-. The average sensitivity of the sensors was 101.9 ± 10.3% at 16.7 mM AcO^- (Figure 5b). The high sensitivity toward AcO^- is attributed to the internal charge transfer as a result of the deprotonation of the thiourea group upon addition of AcO^-.[55,56] In contrast, lower sensitivity transitions were obtained for Cl^- (10.6 ± 0.7%) and Br^- (4.8 ± 4.0%) at 16.7 mM, which reflect their weak hydrogen-bonding interactions with the thiourea group. Negligible sensitivity was observed toward NO_3^-. These sensitivity trends are consistent with the binding studies as confirmed by ^{1}H NMR using model selector **2**. The selectivity of selector **2** can be anticipated based on the basicity of anions, wherein moderately to strongly basic anions that can deprotonate the selector provide the highest sensitivity resistivity changes.[57]

Control studies were performed using as-sprayed P4VP-SWCNT and an ethylated pyridyl group from P4VP-SWCNT without the thiourea group (Figure S13). Pristine P4VP-SWCNT exhibited negligible sensitivity changes toward the anion species (Figure S13a). Noticeable changes were observed with the ethylated P4VP-SWCNT after injection of AcO^- (10.7 ± 2.06%) (Figure 5b and Figure S13b). Nevertheless, ethylated P4VP-SWCNT exhibited a much lower sensitivity as compared to that of P4VP-**2**-SWCNT toward AcO^-, which demonstrates the critical contribution of the thiourea-based dual-hydrogen-bond donor for detection of AcO^-. The ethylated P4VP-SWCNT exhibited insignificant responses toward Cl^-, Br^-, and NO_3^-.

Continuous detection of multiple anions was demonstrated in real-time using three sensor arrays by connecting three resistors in series (in the inset of Figure 5c). Different sensitivity transitions were obtained upon addition of the three anion analytes, wherein the highest sensitivity was achieved toward AcO^- with minor sensitivity to Cl^- and NO_3^- at 16.7 mM. The sensor array can be applied in the rapid screening of biological samples from the individual bacterial cell environment for detection of AcO^- as well as evaluation of AcO^- concentration.[58] The concentration-dependent AcO^- sensitivity was investigated with the P4VP-**2**-SWCNT sensor over the concentration range of 0.17−83.33 mM (Figure 5d). Although longer saturation times were required to stabilize the sensitivity transition with decreasing AcO^- concentrations, a noticeable sensitivity of 25.3% was obtained at 0.83 mM.

The reusability of the P4VP-**2**-SWCNT sensor was investigated by protonation of the sensor upon injection of HBr (0.1 M). As a result, recovery of the initial sensitivity was achieved after protonation of the selector (Figure S14a). In addition, reversible AcO^- detection by deprotonation and subsequent protonation of the P4VP-**2**-SWCNT sensor was demonstrated using the three-sensor array (Figure S14b), which confirms the reusability of the anion-sensing platform. The real-time detection of basic anions such as OH^- is also possible using the P4VP-**2**-SWCNT sensor by facilitating deprotonation of the selector and subsequent electrical transduction upon addition of OH^- anion, which can be applicable in paper pulp, electroplating, and wastewater treatment plants and anion-exchange membrane (AEM) fuel cells.[59,60]

The effect on the AcO^- sensitivity to water was investigated using the P4VP-**2**-SWCNT sensor (Figure S15). Decreased AcO^- sensitivity was observed with increases of the content of water in the sensing environment. Approximately a 35% decrease in sensitivity was observed with 5% water content. In addition, there was a negligible sensory signal at 50% water content. The decreased sensitivity toward AcO^- is attributed to competing hydrogen-bonding interactions with the water solvent.[61,62] For the practical utility of the anion-sensing platform, preparation of analyte samples in an aqueous solution and injection of a minimal amount of sample to the stabilized sensor could be one approach while maintaining minimal water content in the sensing environment. Further development in the design of selectors should be performed for better sensitivity and selectivity in the presence of water while taking advantage of real-time and portable anion-sensing capabilities.

CONCLUSIONS

In summary, we developed real-time anion sensors using a thiourea-based selector functionalized on P4VP-SWCNT for detection of anions in solution (i.e., acetonitrile). The model selectors of **2** and **3** were prepared to investigate the binding affinity toward AcO^-, Cl^-, Br^-, and NO_3^- using ^{1}H NMR and UV−vis titrations. A large change in chemical shift ($\Delta\delta$ = 3.18 ppm) of the N−H proton (H_α) was obtained for **2** upon addition of 3.22 equiv of AcO^- as confirmed by ^{1}H NMR. In addition, selector **2** exhibited a noticeable chemical shift change ($\Delta\delta$ = 0.79 ppm) upon addition of 3.53 equiv of Cl^-. The equilibrium constants (K) of **2** were obtained toward AcO^- (1.99×10^3 M^{-1}) and Cl^- (2.51×10^2 M^{-1}) as calculated from the chemical shift of H_α versus the equivalent of anions. Negligible binding affinities ($\Delta\delta \leq 0.15$ ppm) of **2** to Br^- and NO_3^- resulted in the low equilibrium constants ($K < 15$ M^{-1}). Selector **2** is deprotonated upon addition of AcO^-, whereas Cl^-, Br^-, and NO_3^- formed hydrogen-bonding interactions with **2**. The effect of the cationic moiety on the binding affinity was investigated by comparing selector **2** with selector **3**, wherein the pyridinium group is replaced by a hydroxyl group. Approximately 2.8-fold improved binding affinity toward AcO^- was achieved with selector **2** as compared to selector **3**, which was attributed to the lower pK_a value (11.07 ± 0.11) of **2** than that of selector **3** (pK_a = 11.69 ± 0.07). The anion sensors were fabricated by functionalization of selector **2** on P4VP-SWCNT (P4VP-**2**-SWCNT) by a two-step surface reaction sequence. The sensing results revealed that a large sensitivity change (101.9 ± 10.3%) was achieved after injection of 16.7 mM (2 μL) AcO^-. In addition, real-time detection of multiple anions was demonstrated by continuously monitoring of sensitivity transitions of three-sensor array under the sequential injection of NO_3^-, Cl^-, and AcO^-.

ASSOCIATED CONTENT

Supporting Information

The Supporting Information is available free of charge at https://pubs.acs.org/doi/10.1021/acsami.0c03813.

General materials, characterization, synthesis procedures, NMR spectra, anion binding study, experimental pK_a determination, computational details, fabrication of anion sensor, anion-sensing measurement, additional data, and coordinates of optimized geometries (PDF)

AUTHOR INFORMATION

Corresponding Author

Timothy M. Swager − *Department of Chemistry and Institute for Soldier Nanotechnologies, Massachusetts Institute of Technology, Cambridge, Massachusetts 02139, United States;*

https://dx.doi.org/10.1021/acsami.0c03813
ACS Appl. Mater. Interfaces 2020, 12, 28375−28382

orcid.org/0000-0002-3577-0510; Email: tswager@mit.edu

Authors

Seon-Jin Choi − *Department of Chemistry, Massachusetts Institute of Technology, Cambridge, Massachusetts 02139, United States; Division of Materials of Science and Engineering, Hanyang University, Seoul 04763, Republic of Korea;* orcid.org/0000-0001-8567-0668

Bora Yoon − *Optical and Electromagnetic Materials Team, U.S. Army Combat Capabilities Development Command-Soldier Center (CCDC-SC), Natick, Massachusetts 01760, United States; Institute for Soldier Nanotechnologies, Massachusetts Institute of Technology, Cambridge, Massachusetts 02139, United States*

Sibo Lin − *Department of Chemistry and Institute for Soldier Nanotechnologies, Massachusetts Institute of Technology, Cambridge, Massachusetts 02139, United States*

Complete contact information is available at: https://pubs.acs.org/10.1021/acsami.0c03813

Notes

The authors declare no competing financial interest.

■ ACKNOWLEDGMENTS

This material is based on work supported by the U.S. Army Engineer Research and Development Center Environmental Quality Technology Program under contract W912HZ-17-2-0027 and conducted at Massachusetts Institute of Technology. B.Y. was supported by an appointment to the Postgraduate Research Participation Program at CCDC-SC administered by the Oak Ridge Institute for Science and Education through an interagency agreement between the U.S. Department of Energy and CCDC-SC. This work was supported by the National Research Foundation of Korea (NRF) grant funded by the Korea government (MSIT) (No. 2020R1C1C1010336). S.J.C. thanks Dr. Maggie He [Massachusetts Institute of Technology (MIT)] for helpful discussion about the synthesis of selectors.

■ REFERENCES

(1) Gale, P. A. Anion Receptor Chemistry. *Chem. Commun.* **2011**, *47* (1), 82−86.
(2) Busschaert, N.; Caltagirone, C.; Van Rossom, W.; Gale, P. A. Applications of Supramolecular Anion Recognition. *Chem. Rev.* **2015**, *115* (15), 8038−8155.
(3) Beer, P. D.; Gale, P. A. Anion Recognition and Sensing: The State of the Art and Future Perspectives. *Angew. Chem., Int. Ed.* **2001**, *40* (3), 486−516.
(4) Kim, S.-J.; Choi, S.-J.; Jang, J.-S.; Cho, H.-J.; Kim, I.-D. Innovative Nanosensor for Disease Diagnosis. *Acc. Chem. Res.* **2017**, *50* (7), 1587−1596.
(5) Davis, A. P.; Sheppard, D. N.; Smith, B. D. Development of Synthetic Membrane Transporters for Anions. *Chem. Soc. Rev.* **2007**, *36* (2), 348−357.
(6) Busschaert, N.; Gale, P. A. Small-Molecule Lipid-Bilayer Anion Transporters for Biological Applications. *Angew. Chem., Int. Ed.* **2013**, *52* (5), 1374−1382.
(7) Wolfe, A. J. The Acetate Switch. *Microbiol. Mol. Biol. Rev.* **2005**, *69* (1), 12−50.
(8) Leone, S.; Sannino, F.; Tutino, M. L.; Parrilli, E.; Picone, D. Acetate: Friend or Foe? Efficient Production of a Sweet Protein in Escherichia Coli BL21 Using Acetate as a Carbon Source. *Microb. Cell Fact.* **2015**, *14* (1), 1−10.
(9) De Mey, M.; De Maeseneire, S.; Soetaert, W.; Vandamme, E. Minimizing Acetate Formation in E-coli Fermentations. *J. Ind. Microbiol. Biotechnol.* **2007**, *34* (11), 689−700.
(10) Jia, C. D.; Zuo, W.; Zhang, D.; Yang, X. J.; Wu, B. Anion Recognition by Oligo-(Thio)urea-Based Receptors. *Chem. Commun.* **2016**, *52* (62), 9614−9627.
(11) Huang, H. W.; Xin, Z. H.; Yuan, L.; Wang, B. Y.; Cao, Q. Y. New Ferrocene-Pyrene Dyads Bearing Amide/Thiourea Hybrid Donors for Anion Recognition. *Inorg. Chim. Acta* **2018**, *483*, 425−430.
(12) Nie, L.; Li, Z.; Han, J.; Zhang, X.; Yang, R.; Liu, W. X.; Wu, F. Y.; Xie, J. W.; Zhao, Y. F.; Jiang, Y. B. Development of N-benzamidothioureas As a New Generation of Thiourea-Based Receptors For Anion Recognition and Sensing. *J. Org. Chem.* **2004**, *69* (19), 6449−6454.
(13) Amendola, V.; Fabbrizzi, L.; Mosca, L. Anion Recognition By Hydrogen Bonding: Urea-Based Receptors. *Chem. Soc. Rev.* **2010**, *39* (10), 3889−3915.
(14) Perez-Casas, C.; Yatsimirsky, A. K. Detailing Hydrogen Bonding and Deprotonation Equilibria Between Anions and Urea/Thiourea Derivatives. *J. Org. Chem.* **2008**, *73* (6), 2275−2284.
(15) Li, A. F.; Wang, J. H.; Wang, F.; Jiang, Y. B. Anion Complexation and Sensing Using Modified Urea and Thiourea-Based Receptors. *Chem. Soc. Rev.* **2010**, *39* (10), 3729−3745.
(16) Zahran, E. M.; Hua, Y. R.; Lee, S.; Flood, A. H.; Bachas, L. G. Ion-Selective Electrodes Based on a Pyridyl-Containing Triazolophane: Altering Halide Selectivity by Combining Dipole-Promoted Cooperativity with Hydrogen Bonding. *Anal. Chem.* **2011**, *83* (9), 3455−3461.
(17) Zahran, E. M.; Fatila, E. M.; Chen, C. H.; Flood, A. H.; Bachas, L. G. Cyanostar: C-H Hydrogen Bonding Neutral Carrier Scaffold for Anion-Selective Sensors. *Anal. Chem.* **2018**, *90* (3), 1925−1933.
(18) Buhlmann, P.; Pretsch, E.; Bakker, E. Carrier-Based Ion-Selective Electrodes and Bulk Optodes. 2. Ionophores For Potentiometric and Optical Sensors. *Chem. Rev.* **1998**, *98* (4), 1593−1687.
(19) Bakker, E. Enhancing Ion-Selective Polymeric Membrane Electrodes By Instrumental Control. *TrAC, Trends Anal. Chem.* **2014**, *53*, 98−105.
(20) He, Q.; Vargas-Zuniga, G. I.; Kim, S. H.; Kim, S. K.; Sessler, J. L. Macrocycles as Ion Pair Receptors. *Chem. Rev.* **2019**, *119* (17), 9753−9835.
(21) Zhang, Z.; Kim, D. S.; Lin, C. Y.; Zhang, H. C.; Lammer, A. D.; Lynch, V. M.; Popov, I.; Miljanic, O. S.; Anslyn, E. V.; Sessler, J. L. Expanded Porphyrin-Anion Supramolecular Assemblies: Environmentally Responsive Sensors for Organic Solvents and Anions. *J. Am. Chem. Soc.* **2015**, *137* (24), 7769−7774.
(22) Joyce, L. A.; Shabbir, S. H.; Anslyn, E. V. The Uses of Supramolecular Chemistry in Synthetic Methodology Development: Examples of Anion and Neutral Molecular Recognition. *Chem. Soc. Rev.* **2010**, *39* (10), 3621−3632.
(23) Dahan, A.; Ashkenazi, T.; Kuznetsov, V.; Makievski, S.; Drug, E.; Fadeev, L.; Bramson, M.; Schokoroy, S.; Rozenshine-Kemelmakher, E.; Gozin, M. Synthesis and Evaluation of a Pseudocyclic Tristhiourea-Based Anion Host. *J. Org. Chem.* **2007**, *72* (7), 2289−2296.
(24) Dias, C. M.; Li, H. Y.; Valkenier, H.; Karagiannidis, L. E.; Gale, P. A.; Sheppard, D. N.; Davis, A. P. Anion Transport by Ortho-Phenylene Bis-Ureas Across Cell and Vesicle Membranes. *Org. Biomol. Chem.* **2018**, *16* (7), 1083−1087.
(25) Cox, J. R.; Muller, P.; Swager, T. M. Interrupted Energy Transfer: Highly Selective Detection of Cyclic Ketones in the Vapor Phase. *J. Am. Chem. Soc.* **2011**, *133* (33), 12910−12913.
(26) Pushina, M.; Koutnik, P.; Nishiyabu, R.; Minami, T.; Savechenkov, P.; Anzenbacher, P. Anion Sensing by Fluorescent Expanded Calixpyrroles. *Chem. - Eur. J.* **2018**, *24* (19), 4879−4884.
(27) Bose, P.; Ahamed, B. N.; Ghosh, P. Functionalized Guanidinium Chloride Based Colourimetric Sensors For Fluoride and Acetate: Single Crystal X-Ray Structural Evidence of -NH

Deprotonation and Complexation. *Org. Biomol. Chem.* **2011**, *9* (6), 1972−1979.
(28) Kumar, R.; Jain, H.; Gahlyan, P.; Joshi, A.; Ramachandran, C. N. A Highly Sensitive Pyridine-Dicarbohydrazide Based Chemosensor For Colorimetric Recognition of Cu^{2+}, AMP^{2-}, F^- and AcO^- ions. *New J. Chem.* **2018**, *42* (11), 8567−8576.
(29) Evans, N. H.; Beer, P. D. A Ferrocene Functionalized Rotaxane Host System Capable of the Electrochemical Recognition of Chloride. *Org. Biomol. Chem.* **2011**, *9* (1), 92−100.
(30) Lim, J. Y. C.; Cunningham, M. J.; Davis, J. J.; Beer, P. D. Neutral Redox-Active Hydrogen- and Halogen-Bonding [2]Rotaxanes For the Electrochemical Sensing of Chloride. *Dalton T.* **2014**, *43* (46), 17274−17282.
(31) Takeuchi, M.; Shioya, T.; Swager, T. M. Allosteric Fluoride Anion Recognition By a Doubly Strapped Porphyrin. *Angew. Chem., Int. Ed.* **2001**, *40* (18), 3372−3376.
(32) Zdrachek, E.; Bakker, E. Potentiometric Sensing. *Anal. Chem.* **2019**, *91* (1), 2−26.
(33) Aydogan, A.; Koca, A.; Sener, M. K.; Sessler, J. L. EDOT-Functionalized Calix[4]pyrrole for the Electrochemical Sensing of Fluoride in Water. *Org. Lett.* **2014**, *16* (14), 3764−3767.
(34) Lovering, K.; Nayak, S.; Bu, W.; Uysal, A. The Role of Specific Ion Effects in Ion Transport: The Case of Nitrate and Thiocyanate. *J. Phys. Chem. C* **2020**, *124* (1), 573−581.
(35) Neal, J. F.; Zhao, W.; Grooms, A. J.; Flood, A. H.; Allen, H. C. Arginine-Phosphate Recognition Enhanced in Phospholipid Monolayers at Aqueous Interfaces. *J. Phys. Chem. C* **2018**, *122* (46), 26362−26371.
(36) Liu, Y. J.; Zhao, Z. X.; Huo, R.; Liu, Q. X. Two Macrocycle-Based Sensors For Anions Sensing. *Sci. Rep.* **2019**, *9*, 502.
(37) Farshbaf, S.; Anzenbacher, P. Fluorimetric Sensing of ATP in Water By an Imidazolium Hydrazone Based Sensor. *Chem. Commun.* **2019**, *55* (12), 1770−1773.
(38) Lim, J. Y. C.; Marques, I.; Thompson, A. L.; Christensen, K. E.; Felix, V.; Beer, P. D. Chalcogen Bonding Macrocycles and [2]Rotaxanes for Anion Recognition. *J. Am. Chem. Soc.* **2017**, *139* (8), 3122−3133.
(39) Bergamaschi, G.; Boiocchi, M.; Monzani, E.; Amendola, V. Pyridinium/Urea-Based Anion Receptor: Methine Formation in the Presence of Basic Anions. *Org. Biomol. Chem.* **2011**, *9* (24), 8276−8283.
(40) Fechner, L. E.; Albanyan, B.; Vieira, V. M. P.; Laurini, E.; Posocco, P.; Pricl, S.; Smith, D. K. Electrostatic Binding of Polyanions Using Self-Assembled Multivalent (SAMul) Ligand Displays-Structure-Activity Effects on DNA/Heparin Binding. *Chem. Sci.* **2016**, *7* (7), 4653−4659.
(41) Chan, C. W.; Laurini, E.; Posocco, P.; Pricl, S.; Smith, D. K. Chiral Recognition at Self-Assembled Multivalent (SAMul) Nanoscale Interfaces - Enantioselectivity in Polyanion Binding. *Chem. Commun.* **2016**, *52* (69), 10540−10543.
(42) Gale, P. A.; Caltagirone, C. Fluorescent and Colorimetric Sensors For Anionic Species. *Coord. Chem. Rev.* **2018**, *354*, 2−27.
(43) Schroeder, V.; Savagatrup, S.; He, M.; Lin, S.; Swager, T. M. Carbon Nanotube Chemical Sensors. *Chem. Rev.* **2019**, *119* (1), 599−663.
(44) Frazier, K. M.; Swager, T. M. Robust Cyclohexanone Selective Chemiresistors Based on Single-Walled Carbon Nanotubes. *Anal. Chem.* **2013**, *85* (15), 7154−7158.
(45) Yoon, B.; Liu, S. F.; Swager, T. M. Surface-Anchored Poly(4-vinylpyridine)-Single-Walled Carbon Nanotube Metal Composites for Gas Detection. *Chem. Mater.* **2016**, *28* (16), 5916−5924.
(46) Zhu, R.; Desroches, M.; Yoon, B.; Swager, T. M. Wireless Oxygen Sensors Enabled by Fe(II)-Polymer Wrapped Carbon Nanotubes. *ACS Sens.* **2017**, *2* (7), 1044−1050.
(47) Yoon, B.; Choi, S. J.; Swager, T. M.; Walsh, G. F. Switchable Single-Walled Carbon Nanotube-Polymer Composites for CO_2 Sensing. *ACS Appl. Mater. Interfaces* **2018**, *10* (39), 33373−33379.
(48) Choi, S. J.; Yoon, B.; Ray, J. D.; Netchaev, A.; Moores, L. C.; Swager, T. M. Chemiresistors for the Real-Time Wireless Detection of Anions. *Adv. Funct. Mater.* **2020**, *30* (7), 1907087.
(49) Farrugia, K. N.; Makuc, D.; Podborska, A.; Szacilowski, K.; Plavec, J.; Magri, D. C. UV-Visible and ^{1}H-^{15}N NMR Spectroscopic Studies of Colorimetric Thiosemicarbazide Anion Sensors. *Org. Biomol. Chem.* **2015**, *13* (6), 1662−1672.
(50) Amendola, V.; Bergamaschi, G.; Boiocchi, M.; Fabbrizzi, L.; Milani, M. The Squaramide versus Urea Contest for Anion Recognition. *Chem. - Eur. J.* **2010**, *16* (14), 4368−4380.
(51) Elmes, R. B. P.; Turner, P.; Jolliffe, K. A. Colorimetric and Luminescent Sensors for Chloride: Hydrogen Bonding vs Deprotonation. *Org. Lett.* **2013**, *15* (22), 5638−5641.
(52) Jeppesen, A.; Nielsen, B. E.; Larsen, D.; Akselsen, O. M.; Solling, T. I.; Brock-Nannestad, T.; Pittelkow, M. Croconamides: A New Dual Hydrogen Bond Donating Motif for Anion Recognition and Organocatalysis. *Org. Biomol. Chem.* **2017**, *15* (13), 2784−2790.
(53) Li, B. L.; Lu, X. L.; Ma, Y. H.; Chen, Z. Thermo- and pH-Responsive Behaviors of Aqueous Poly(acrylic acid)/Poly(4-vinylpyridine) Complex Material Characterized by ATR-FTIR and UV-Vis Spectroscopy. *Eur. Polym. J.* **2014**, *60*, 255−261.
(54) Khan, S. I.; Ali Khan, I.; Badshah, A.; Perveen Malik, F.; Tabassum, S.; Ullah, I.; Zargarian, D.; Khawar Rauf, M. Mononuclear Copper(I) Complexes with Triphenylphosphine and N,N'-disubstituted Thioureas: Synthesis, Characterization, and Biological Evaluation. *J. Coord. Chem.* **2018**, *71* (24), 4086−4108.
(55) Boiocchi, M.; Del Boca, L.; Gomez, D. E.; Fabbrizzi, L.; Licchelli, M.; Monzani, E. Nature of Urea-Fluoride Interaction: Incipient and Definitive Proton Transfer. *J. Am. Chem. Soc.* **2004**, *126* (50), 16507−16514.
(56) Gomez, D. E.; Fabbrizzi, L.; Licchelli, M.; Monzani, E. Urea vs. Thiourea in Anion Recognition. *Org. Biomol. Chem.* **2005**, *3* (8), 1495−1500.
(57) Vargas-Zuniga, G. I.; Sessler, J. L. Pyrrole N-H Anion Complexes. *Coord. Chem. Rev.* **2017**, *345*, 281−296.
(58) Carey, J. R.; Suslick, K. S.; Hulkower, K. I.; Imlay, J. A.; Imlay, K. R. C.; Ingison, C. K.; Ponder, J. B.; Sen, A.; Wittrig, A. E. Rapid Identification of Bacteria with a Disposable Colorimetric Sensing Array. *J. Am. Chem. Soc.* **2011**, *133* (19), 7571−7576.
(59) Irkham; Einaga, Y. Oxidation of hydroxide ions in weak basic solutions using boron-doped diamond electrodes: effect of the buffer capacity. *Analyst* **2019**, *144* (15), 4499−4504.
(60) Cao, X. Z.; Novitski, D.; Holdcroft, S. Visualization of Hydroxide Ion Formation upon Electrolytic Water Splitting in an Anion Exchange Membrane. *ACS Mater. Lett.* **2019**, *1* (3), 362−366.
(61) Langton, M. J.; Serpell, C. J.; Beer, P. D. Anion Recognition in Water: Recent Advances from a Supramolecular and Macromolecular Perspective. *Angew. Chem., Int. Ed.* **2016**, *55* (6), 1974−1987.
(62) Kubik, S. Anion recognition in water. *Chem. Soc. Rev.* **2010**, *39* (10), 3648−3663.

https://dx.doi.org/10.1021/acsami.0c03813
ACS Appl. Mater. Interfaces 2020, 12, 28375−28382